Unified Mechanistic Understanding of CO_2 Reduction to CO on Transition Metal and Single Atom Catalysts

*Sudarshan Vijay[1], Wen Ju[2], Sven Brückner[2], Peter Strasser[2], Karen Chan[1]**

AUTHOR ADDRESS

1. *CatTheory, Department of Physics, Technical University of Denmark, 2800 Kgs. Lyngby, Denmark*
2. *Department of Chemistry, Chemical Engineering Division, Technical University Berlin, Berlin 10623, Germany*

**kchan@fysik.dtu.dk*

TOC Image

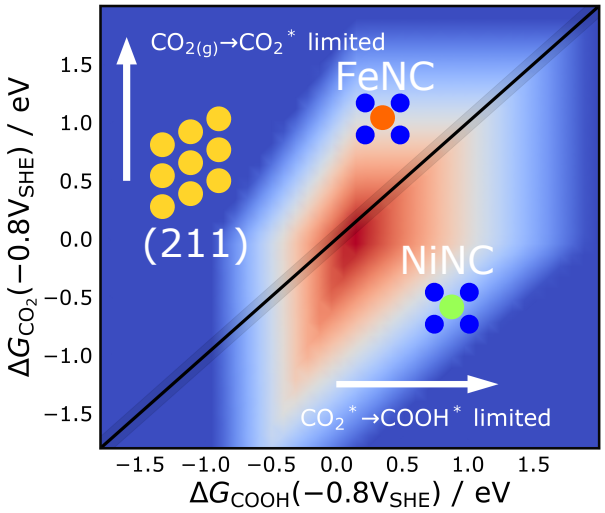

Abstract

CO is the simplest product from CO_2 electroreduction (CO_2R), but the identity and nature of its rate limiting step remains controversial. Here we investigate the activity of both transition metals (TMs) and metal-nitrogen doped carbon catalysts (MNCs), and a present unified mechanistic picture of CO_2R to CO for both these classes of catalysts. By consideration of the electronic structure through a Newns-Andersen model, we find that on MNCs, like TMs, electron transfer to CO_2 is facile, such that CO_2(g) adsorption is driven by adsorbate dipole-field interactions. Using density functional theory with explicit consideration of the interfacial field, we find CO_2* adsorption to generally be limiting on TMs, while MNCs can be limited by either CO_2* adsorption or by the proton-electron transfer reaction to form COOH*. We evaluate these computed mechanisms against pH-dependent experimental activity measurements on CO_2R to CO activity for Au, FeNC, and NiNC. We present a unified activity volcano that, in contrast to previous

analyses, includes the decisive CO_2* and COOH* binding strengths as well as the critical adsorbate dipole-field interactions. We furthermore show that MNC catalysts are tunable towards higher activity away from transition metal scaling, due to the stabilization of larger adsorbate dipoles resulting from their discrete and narrow *d*-states. The analysis suggests two design principles for ideal catalysts: moderate CO_2* and COOH* binding strengths as well as large dipoles on the CO_2* intermediate. We suggest that these principles can be exploited in materials with similar electronic structure to MNCs, such as supported single-atom catalysts, molecules, and nanoclusters, 2D materials, and ionic compounds towards higher CO_2R activity. This work captures the decisive impact of adsorbate dipole-field interactions in CO_2R to CO and paves the way for computational-guided design of new catalysts for this reaction.

Introduction

Electrochemical reduction of CO_2 (CO_2R) has the potential to store renewable energy in the form of high value chemicals.[1–3] The simplest product obtained during the reduction of CO_2 is CO, which can be used as a renewable feedstock for the Fischer-Tropsch reaction.[4] This process is also the first CO_2R reaction to be realized commercially, with Ag gas-diffusion electrodes that yield up to 300 mAcm^{-2} of CO towards the production of polymers.[5] Nanostructured forms of gold and silver are currently the state-of-the-art catalysts for this reaction. Aside from their cost, these transition metal (TM) catalysts also catalyze the competing hydrogen evolution reaction (HER), which reduces the selectivity to CO. A recently proposed alternative for CO_2R to CO is metal and nitrogen doped carbon (MNC), which is low-cost, earth-abundant.[6] These catalysts also have the advantage that they are less selective towards HER than TM catalysts, with Faradaic efficiencies of H_2 of less

than 20% under typical operating conditions of -0.6 V vs RHE,[7,8] consistent with the scaling of the H* and CO* binding energies on these materials.[6]

CO_2R to CO requires two proton-electron transfers. In acid:

$$CO_2(g) + 2H^+ + e^- \rightarrow CO(g) + H_2O(l).$$

Despite its apparent simplicity, its mechanism remains debated in recent work. Firstly, the rate limiting step has been proposed to be CO_2 adsorption on Au,[9,10] Fe and Ni doped MNC catalysts (FeNC, NiNC),[8,11] $COOH*$ formation on noble metals,[12,13] or $COOH*$ to CO(g) on Ag from $C-O$ bond breaking.[14] Tafel slopes of 60 or 120 mV/dec are sometimes taken as indicators of certain rate-limiting steps;[9,12] however, a recent comprehensive analysis of existing data shows silver, gold, copper, zinc and tin catalysts to have no intrinsic preference for such "cardinal values", consistent with models of electron transfer in electrochemistry.[15]

Furthermore, the nature of the CO_2 adsorption step is a source of some controversy. $CO_2(g)$ adsorption was suggested to give rise to a unit-charged CO_2^- species on both Au[16,17] and FeNC catalysts, not treatable with ground-state DFT methods.[18] This hypothesis may originate from the reduction process of $CO_{2(aq)}$ to a $CO_{2(aq)}^-$ that occurs at extremely negative potentials of -1.9 V vs. SHE,[19] or from homogeneous catalysis.[20,21] Solvent reorganization, as first considered through Marcus theory, has also been hypothesized to be a major contributor to the energetics of CO_2 adsorption.[17,22] Alternatively, it has been proposed that CO_2* adsorption is driven by the interaction of the dipole of CO_2* with the interfacial electric field;[23,24] given facile electron transfer on metals, there is no distinct, extra-charged "CO_2^-" species vs. a polarized CO_2* adsorbate, no

different from any other surface adsorbate such as CO*, OH*, for example.[25] The CO_2* dipole has similarly been described in terms of a partial charge transfer from the metal to adsorbate.[11,26]

In this work, we present a unified mechanistic picture of CO_2R to CO on both these classes of catalysts. By consideration of the width of adsorbate induced density of states, we find that on MNCs, like TMs, electron transfer to CO_2 is extremely facile, such that a field-driven, CO_2 adsorption step is treatable with standard ground state DFT methods. Using DFT with explicit consideration of adsorbate-field interactions, we find CO_2* formation to generally be limiting on TMs, while MNCs can be limited by either CO_2* adsorption or COOH* formation. We evaluate these computed mechanisms against pH-dependent activity measurements on CO_2R to CO activity for Au, FeNC, and NiNC. We present a unified kinetic activity volcano with CO_2* and COOH* binding strengths as the descriptors, reflecting how the formation of either can be rate limiting, and with consideration of the decisive adsorbate-dipole interactions. We furthermore show that MNC catalysts are tunable towards higher activity away from transition metal scaling, due to the stabilization of larger CO_2* dipoles that result from narrower metal *d*-states. We discuss the implications of these findings for catalyst design, i.e. the optimization of the CO_2* dipole is a critical descriptor in addition to the adsorption energies of key intermediates.

Electron transfer is not rate limiting on MNC catalysts

Previous reports have proposed the formation of a CO_2^- state as the rate limiting step for CO_2R to CO. This step has been suggested to be limited by solvent reorganization[22,27] or by electron transfer to an uncharged CO_2* state to give an excited, charged CO_2^- state, which cannot be modelled with

workhorse, ground-state periodic DFT methods.[18] Below we show that electron transfer to adsorbates is not limiting (and therefore adiabatic) on MNC catalysts, which allows us to determine the CO_2R energetics with computing the one and only CO_2* state using conventional, periodic DFT along with the application of a stabilizing surface charge.

As in Ref.[28] for an Au surface, we determine the rate of electron hopping between the s,p states of the adsorbate and the states of the surface, k. We compare this rate against concurrent processes such as adsorbate diffusion to the surface. If the timescale for the electron transfer is very small in comparison, it will not be rate limiting to species like CO_2* and we would only need to consider the adiabatic pathway for CO_2 adsorption. In the Newns-Anderson[29–31] model of chemisorption, the width of adsorbate induced states is $\Delta = \Sigma_k |V_{ak}|^2 \delta(\epsilon_a - \epsilon_k)$, V_{ak} is the coupling matrix element between k and individual s, p states, ϵ_a are the single particle energies of the adsorbate s,p states and ϵ_k is the energy of the surface states. Δ can be determined from the projected density of states (PDOS) onto s,p states of CO_2, through the width of the peak at the Fermi level.[28] We obtain the rate of electron transfer from Fermi's Golden Rule, $\frac{2\pi}{\hbar}\Delta$. To illustrate this idea, **Figure 1**a shows the rates of electron transfer associated with a range of idealized peaks of different width, shown in **Figure 1**b. For a very small width of 0.1 eV, the rate of electron hopping is extremely fast, greater than 10^{14} s^{-1}, and is larger with increased broadening. For comparison, an estimate for the diffusion rate of ions in solution is of the order 10^{12} s^{-1}, shown by the dashed line.[32]

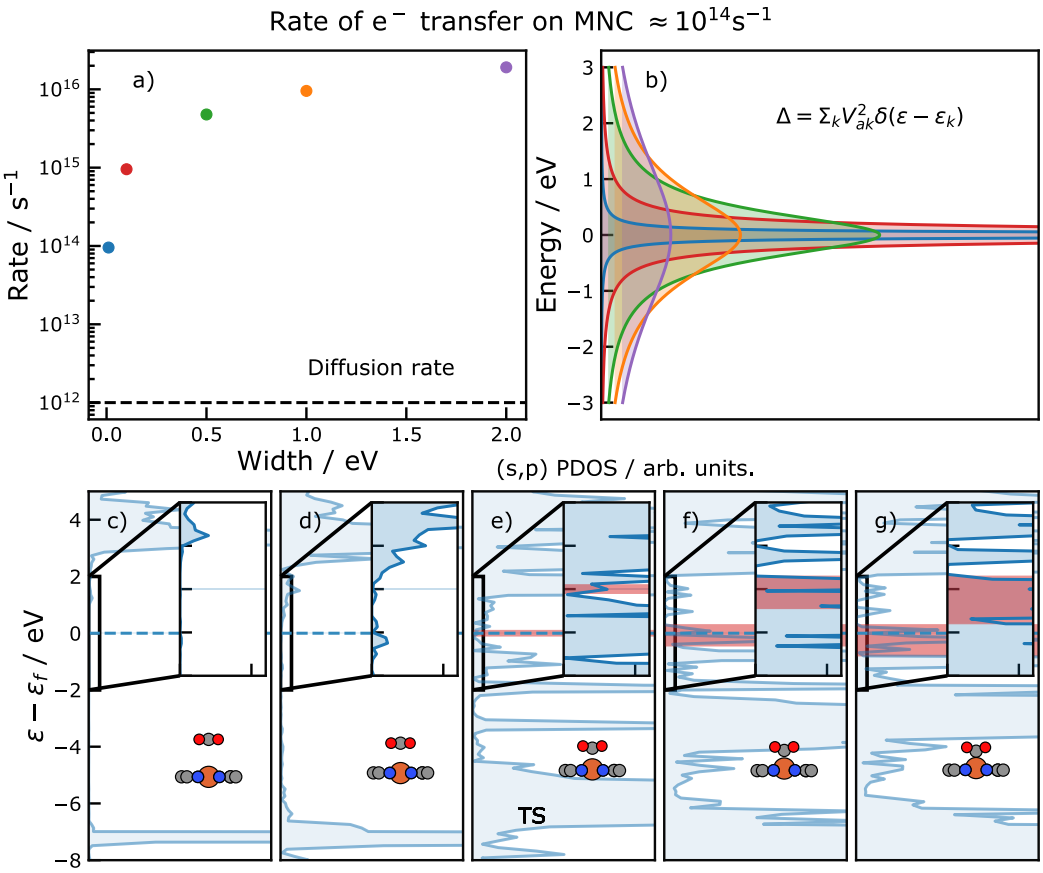

Figure 1: a) Rate of electron hopping for different idealized Lorentzian peaks shown in b). Density of states projected onto CO_2 (s,p) states for (c-g) FeNC show short timescale of electron transfer on FeNC; panels denote select images of a ci-NEB ; red bands indicate estimated width of the of the states at the Fermi level

We now apply this methodology to PDOS obtained from DFT computations. **Figure 1**(c-g) shows the PDOS for the reaction path of CO_2 adsorption on FeN_4 (a prototype for MNC). The s,p states of CO_2 broaden as it approaches the surface, which is expected for adsorption processes in general.[33] At the transition state (TS) and further along the reaction pathway, the peaks at the Fermi level are greater than 0.1 eV. The corresponding rate of electron transfer is approximately $10^{14}s^{-1}$, which implies a timescale of $10^{-14}s$. This rate is in turn two orders of magnitude greater than competing processes which implies that it will not be rate limiting on FeN_4. Since the states at the Fermi level on MNC catalysts are typically the s,p states of graphene (see **SI Note 2**), we expect

this analysis to hold for all MNC catalysts. Thus, only the adiabatic pathway for CO_2 adsorption needs to be calculated in order to obtain the energetics for all elementary steps on MNC and TM catalysts.

We do not exclude the possibility here that solvent reorganization could contribute to the energetics of the CO_2 adsorption step, as has been considered in Ref.[17]. The magnitude of this contribution, however, has been estimated to be only ~0.2 eV from the timescale of reorganization.[34,35] Recent investigations based on the Marcus-Hush-Chidsey model suggest that it can be up to 0.6 eV in the presence of certain electrolytes.[36]

Field-dependent DFT simulations and pH-dependent measurements show both CO_2* adsorption and COOH* formation can be rate limiting

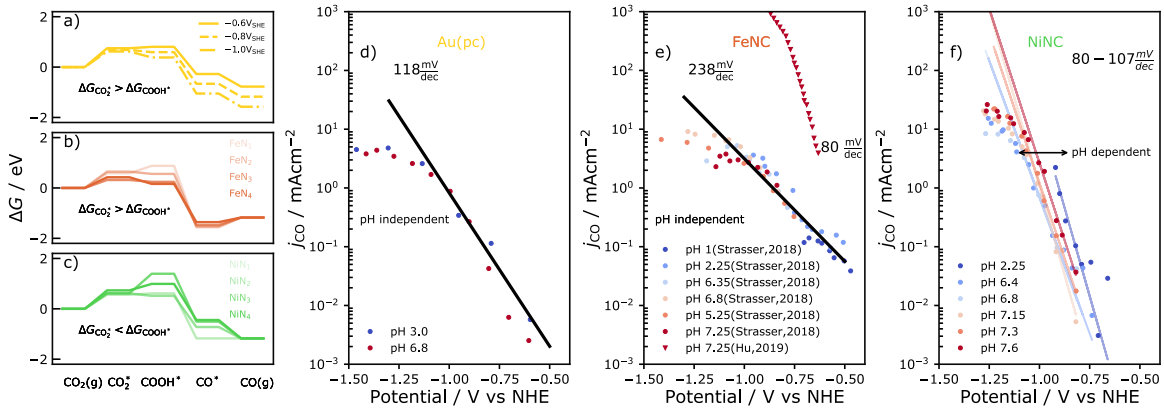

Figure 2: Free energy diagram of $CO_2$to CO for a) Au(211) at U $= -0.6, -0.8$ and -1.0 V_{SHE} b) FeNC c) NiNC in double vacancies with different nitrogen coordination at $U = -0.8V_{SHE}$ with pH = 2. Experimental current densities plotted against NHE potential for d) poly-crystalline Au (from Ref[23]) e) FeNC (from Ref[8] and Ref[37]) f) NiNC (this work)

We now present the mechanism and rate limiting step for Au, FeNC and NiNC determined from potential-dependent DFT calculations and evaluate them against pH-dependent activity measurements. We consider the following reaction pathway (written for acid solutions),

$$CO_2(g) + * \rightarrow CO_2^*$$

$$CO_2^* + H^+ + e^- \rightarrow COOH^*$$

$$COOH^* + H^+ + e^- \rightarrow CO^* + H_2O(g)$$

$$CO^* \rightarrow CO(g) + *$$

We assume here that the barriers associated with all steps are small. As evaluated in Ref.[24] for FeN_2 and FeN_4, the CO_2 adsorption barrier is well approximated by the adsorption energy (differences between barrier and reaction energies of at most 0.2 eV), the protonation of CO_2* is facile, and the $COOH*$ to $CO*$ step for CO producing catalysts is generally so downhill that the corresponding barriers are unlikely to be limiting. The rate limiting step at a given potential is in this case determined by the state with the highest free energy, ΔG. Each ΔG derives its potential dependence either from the presence of a proton-electron pair as reactants and/or from the interaction between the dipoles of participating reaction intermediates with the interfacial field. The energetic response caused by the interaction of a dipole, μ with an interfacial field , ξ is -$\mu\xi$.[38] At reducing potentials, fields set up by the double layer can be as large as 10^{10} V/m, which give rise a significant stabilization of CO_2* on MNCs of $0.75 - 1$ eV on MNCs (see **SI Note 1** for detailed information about methodology used). **Figure 2**a shows the free energy diagram for Au(211) at $-0.6, -0.8$ and $-1 V_{SHE}$, at a pH of 2. At $-0.6 V_{SHE}$, $COOH*$ is the intermediate with the highest ΔG, while at $-0.8 V_{SHE}$ and $-1 V_{SHE}$, it is CO_2*. Thus, the computations predict a

change in rate limiting step from COOH* formation to CO_2* adsorption, when the overpotential is increased, in line with previous work.[23]

We evaluate the rate limiting step with pH dependent measurements. The activity is pH dependent on an absolute scale (e.g. vs. the SHE or NHE) when COOH* formation is rate limiting, since a proton-electron transfer is involved. CO_2* adsorption, on the other hand, does not involve a proton-electron transfer, so when it is rate limiting, the activity is pH independent on an absolute scale. **Figure 2**d shows the measured current densities vs. potential on an NHE scale. The current densities show no pH dependence at high potentials (greater than -0.8 V_{SHE}). At lower overpotentials, the scatter in the points could be indicative of COOH* formation being the rate limiting step.

With the same arguments, we show that FeNC catalysts are limited by the energetics of CO_2* adsorption while NiNC catalysts are limited by the CO_2* → COOH* step. **Figure 2**b shows the free energy diagram for FeNC catalysts computed at $-0.8V_{SHE}$ and a pH of 2 for various nitrogen coordination around the metal center for double vacancies (DV) (metals on single vacancies tend to overbind CO*, see below). For FeN_2, FeN_3 and FeN_4, the computations predict CO_2* adsorption to be rate limiting for potentials more cathodic of -0.8 V_{SHE}, which is in line with the completely pH independent experimental rates (**Figure 2**e, Strasser data). The FeN_4 vacancy configuration has also been stipulated to be the active site for CO_2R based on a comparison of the cyclic voltammograms and x-ray spectral features with molecular analogues.[39] In contrast, FeN_1 is limited by COOH* formation at this potential, and the lack of pH-dependence in experiments suggests that its population on the catalyst surface is small. All NiNC catalysts investigated in

Figure 2c, except for NiN_2, are limited by COOH* formation, consistent with the pH dependence of experimental rates as shown in **Figure 2**f (see **SI Note 3** for total currents and faradaic efficiencies). Thus, the combination of simple field-dependent thermodynamic computations and pH dependent measurements suggests CO_2* adsorption to be rate limiting at higher overpotentials on Au and for all potentials on FeNC, and $CO_2* \rightarrow COOH*$ to be rate limiting on NiNC.

Finally, the experimental Tafel slopes do not show "cardinal values" of 60 or 120mV/dec, as was shown by a comprehensive study of recent literature.[15] These slopes reflect the magnitude of the dipole ($slope^{-1} \sim \frac{C}{\epsilon}\,\mu$, where C is the capacitance)[23,24] and/or the symmetry factor ($0< \alpha <1$) of the associated proton-electron transfer and therefore are not constrained to these values. **Figure 1**e shows that different types of FeNC catalysts from Refs.[8,37] show different Tafel slopes.

The general activity volcano for CO production is determined by both the COOH* and CO_2* adsorption energies

In this section we consolidate the mechanistic insights into a general kinetic activity volcano for CO_2R to CO determined by two activity descriptors, the free energy of adsorption of CO_2, ΔG_{CO_2}, and that of COOH, ΔG_{COOH}. **Figure 3**a shows this unified activity volcano for CO production for both TM and MNC catalysts corresponding to the energetics in **Figure 2**. The theoretical maximum in activity (represented by the turnover frequency, TOF) occurs at intermediate ΔG_{CO_2} and $\Delta G_{COOH} \sim 0$, i.e. where both CO_2 and COOH formation steps are facile. The parity line corresponds to the case where the free energy of COOH* and CO_2* are equal, $\Delta G_{CO_2} = \Delta G_{COOH}$. The CO adsorption energy generally scales with those of the other two intermediates;[40] thus, its

energetics are included in the volcano through the calculated scaling relationships in the kinetic model (see **SI Note 4**).

Figure 3a shows several trends in the binding of CO_2R intermediates for TMs and MNCs. Firstly, the TMs show a scaling line (the dashed black line) between ΔG_{CO_2} and ΔG_{COOH}, while the MNCs show more scatter. Furthermore, metals doped into single vacancies (SV) tend to bind reaction intermediates stronger than double vacancies (DV), and are poisoned by CO. **Figure 3** (a,b) also allows us to determine which step is rate limiting in CO_2R to CO at any given potential, using computed CO_2*, COOH* and CO* free energies. On **Figure 3**a, if the point lies below the parity line, then $CO_2 * \rightarrow COOH *$ is the rate limiting step. Meanwhile, if it is above the parity line, CO_2 adsorption is rate limiting. At very negative adsorption energies, the surface is poisoned by CO as shown in **Figure 3**b, which leads to CO* desorption being rate limiting on TMs such as Pd and Pt. All TM (211) facets lie above the parity line, indicating that CO_2 adsorption or CO desorption is rate limiting at the studied potentials. Some NiNC catalysts lie below the parity line, showing that $CO_2 * \rightarrow COOH *$ is rate limiting, in line with the experimental finding in **Figure 2**f. Note that our approach, in contrast to Ref.[13], includes the effects of the adsorbate-field interactions for all intermediates (see **SI Note 1**) and the consideration of CO_2 adsorption as an elementary step, and these effects are critical to determining the activity trends. **SI Note 4** also shows the potential dependence vs. SHE of the rate map shown in **Figure 3**a.

We generally do not expect there to be a only single site motif present following the synthesis procedure for these materials.[41–44] Temperature programmed desorption experiments (**Figure S9 and SI Note 5**) shows FeNC, but not NiNC, to have a peak above 300K. This result suggests

strong binding sites like those from SV to be present on Fe to a greater extent than NiNC.[45] Note that doped SV sites, or other binding sites of similar binding strength that we haven't considered, are not active sites for CO_2R, as they would be poisoned by CO.

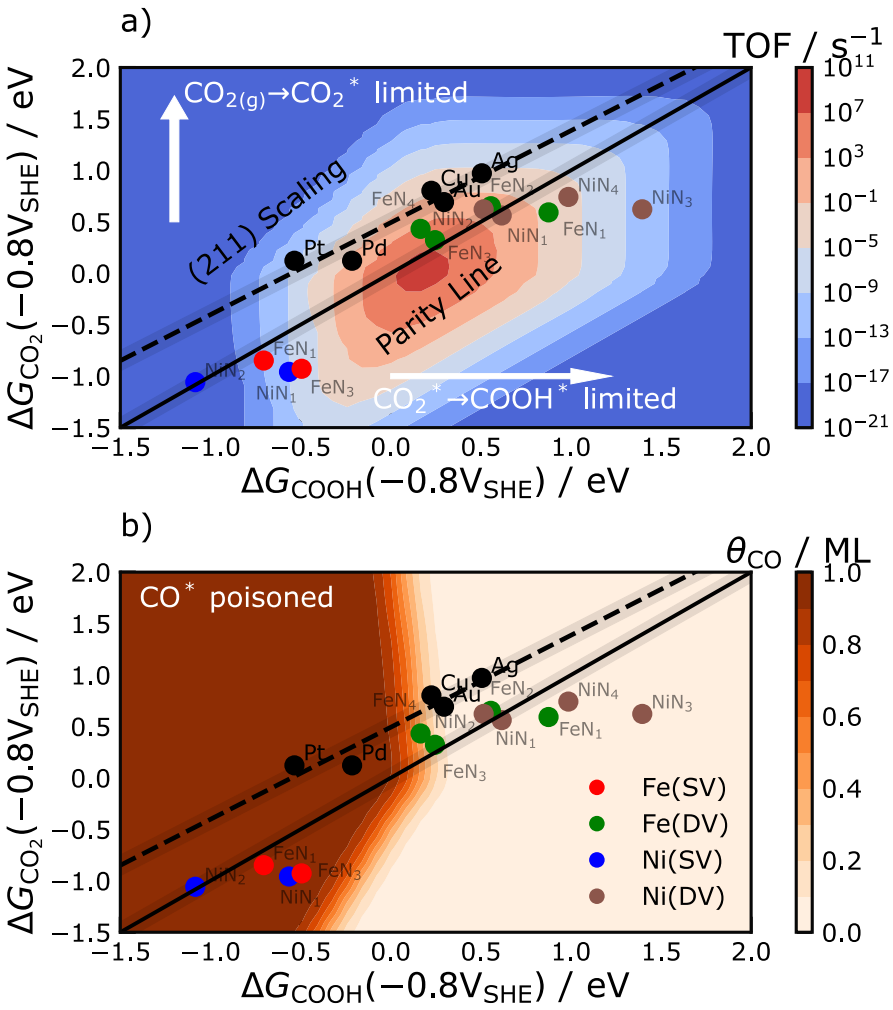

Figure 3: a) Rate map at -0.8 V_{SHE} and pH 2 for CO_2R to CO obtained from the (211) transition metal scaling line, annotated points show MNCs either at single vacancies (SV) or double vacancies (DV) ; (211) scaling line has the best fit $\Delta G_{CO_2} = 0.94\Delta G_{COOH} + 0.51$ b) coverage map with the same points showing which surfaces are poisoned by CO

MNCs deviate from TM scaling in the direction of higher activity, because they stabilize larger dipoles on CO_2*

We now show that MNCs deviate from TM scaling because they stabilize large dipole moments on CO_2*. **Figure 4**b shows charge density difference isosurfaces for CO_2* on Ni_4NC, which shows a perturbation of the electron density near the surface upon adsorption. This change in electron density is captured by the dipole moment, given by $\mu = \int \rho dz$, where ρ is the charge density and z is the axis of integration and is shown in **Figure 4**a for (211) and (100) TM surfaces as well as Fe- and Ni- doped MNC catalysts in both single and double vacancies of various N-concentrations (notation: M(vacancy type, number of coordinating N). The figure shows that the dipole moments for CO_2* are larger than for other adsorbates such as CO* and COOH*. Furthermore, the CO_2* dipoles are significantly higher on MNCs than TMs. MNCs therefore have CO_2* adsorption energies that are stabilized more at reducing potentials where the surface is generally negatively charged. This electrostatic stabilization caused by the dipole-field interaction gives rise to the offset of MNCs from TM scaling line shown in **Figure 3**.

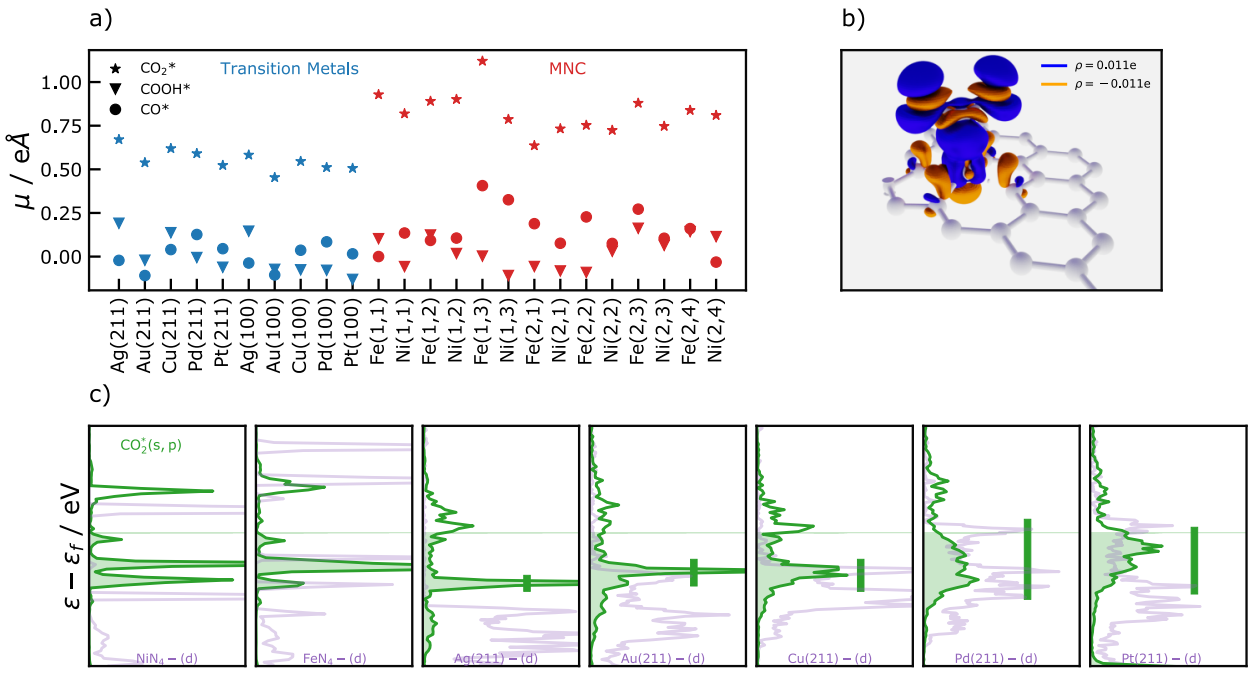

Figure 4: a) Vacuum dipole moments for (211) and (100) TM surfaces and Fe and Ni MNCs; the MNCs have larger dipole moments as compared to TMs; b) charge density difference plot for CO_2 adsorbed on NiN_4C c) Density of states projected onto CO_2* and transition metals show that the adsorbate states are much narrower on MNCs than on TMs

We rationalize the differences in dipole moments with the PDOS on s,p states of CO_2* . The strength of the adsorbate-surface interaction is determined by both the position and shape of the *d*-states, and is reflected in the width of the adsorbate states.[46] As shown in **Figure 4**c for a selected set of surfaces (in green), the width of the s,p states increases in the order FeN_4 and NiN_4 , Ag and Au, and Pd and Pt (metal d-states are shown in purple). In the case of the MNC catalysts and Ag and Au, the sharper the s,p-states of CO_2* mean they resemble those of their molecular counterpart, which indicates a weak interaction (poor hybridization) with the surface. This poor hybridization between CO_2 and the surface means CO_2* retains a greater charge polarization between its two poles, i.e. a larger dipole. Conversely, in the case of Pt and Pd, the broadened states indicate a large interaction.[29] A lower charge polarization results from the mixing of adsorbate states with those

of the surface and a lower resultant surface dipole. Overall, the trends in the width of the s,p PDOS of CO_2* are consistent with the larger dipole moments of MNC catalysts.

The activity volcano of **Figure 3** and electronic structure arguments of **Figure 4** gives two simple design principles. As shown in the TOF of **Figure 3**, the ideal CO_2R catalyst has moderate ΔG_{CO_2} and ΔG_{COOH} of $0.25 - 0.5$ eV and $\Delta G_{CO} > 0$ eV (to prevent CO* poisoning). It must, additionally, be able to stabilize a large dipole moment of CO_2*, such that CO_2 adsorption does not require a significant overpotential (thereby deviating from the scaling of TMs in the direction of higher activity, shown in **Figure 3**). These larger dipole moments are stabilized for MNC catalysts materials through their narrow *d*-states. We suggest that other materials that have similar discrete and narrow *d*-states, such as supported single atoms,[47,48] molecules and clusters,[49,50] as well as 2D materials and ionic compounds,[51–53] could also be active CO_2R catalysts, provided that hydrogen evolution is not competitive or suppressed through a decrease in water activity.[54] This principle could also be relevant for other processes where dipole-field interactions are decisive, such as in C_2 product formation.[4,55]

Conclusion

In summary, we presented a unified picture of the CO_2R to CO on both TM and MNC catalysts that resolves existing controversies on the identity and nature of the rate limiting step. Considering the widths of projected densities of states of an adsorbing CO_2, we showed that, like on TMs, electron transfer to CO_2 is not limiting in MNCs, and such that CO_2 adsorption is driven by adsorbate dipole-field interactions. With a combination of field-dependent DFT and pH-dependent activity measurements, we showed that CO_2* adsorption is limiting on TMs over relevant

potentials, while either CO_2* adsorption or COOH* formation is rate limiting on MNCs. We presented a unified kinetic activity volcano, based on critical COOH* and CO_2* binding as descriptors, that accounts for the decisive adsorbate dipole-field interactions. The volcano shows that ideal catalysts should have both a moderate binding strength of COOH* and CO_2*, as well as large adsorbate dipoles on CO_2*. We furthermore showed that MNCs deviate favorably from TM scaling through the stabilization of large CO_2* dipoles, due to the localized, narrow *d*-states of these materials.

These results suggest that MNCs or other materials with similarly narrow *d*-states such as supported single atoms, molecules and clusters, as well as 2D materials and ionic compounds can be optimized for large dipoles and correspondingly higher catalytic activity beyond transition metal scaling. This principle can be relevant for other processes where adsorbate-field interactions are decisive. The presented kinetic activity volcano and catalyst design rules should be used as the basis for computation-guided catalyst development of CO_2R to CO catalysts.

Acknowledgements

The research leading to these results has received funding from the European Union's Horizon 2020 research and innovation programme under grant agreement No 851441, SELECTCO2. Research leading to some of these results has received funding from the Fuel Cells and Hydrogen 2 Joint Undertaking under grant agreement no. 779366, CRESCENDO. The authors thank Dr. Georg Kastlunger for helpful discussions.

Data and Code Availability

All DFT calculations will be made available at https://data.dtu.dk/ upon publication.

References

1. Jouny, M., Luc, W. & Jiao, F. General Techno-Economic Analysis of CO2 Electrolysis Systems. *Ind. Eng. Chem. Res.* **57**, 2165–2177 (2018).
2. Seh, Z. W. *et al.* Combining Theory and Experiment in Electrocatalysis: Insights into Materials Design. *Science (80-.).* **355**, (2017).
3. Anastasiadou, D., Hensen, E. J. M. & Figueiredo, M. C. Electrocatalytic synthesis of organic carbonates. *Chem. Commun.* **56**, 13082–13092 (2020).
4. Nitopi, S. *et al.* Progress and Perspectives of Electrochemical CO2 Reduction on Copper in Aqueous Electrolyte. *Chem. Rev.* **119**, 7610–7672 (2019).
5. Haas, T., Krause, R., Weber, R., Demler, M. & Schmid, G. Technical photosynthesis involving CO2 electrolysis and fermentation. *Nat. Catal.* **1**, 32–39 (2018).
6. Bagger, A., Ju, W., Varela, A. S., Strasser, P. & Rossmeisl, J. Single Site Porphyrine-like Structures Advantages over Metals for Selective Electrochemical CO2 Reduction. *Catal. Today* **288**, 74–78 (2017).
7. Clark, E. L. *et al.* Influence of Atomic Surface Structure on the Activity of Ag for the Electrochemical Reduction of CO 2 to CO. *ACS Catal.* **9**, 4006–4014 (2019).
8. Varela, A. S. *et al.* PH Effects on the Selectivity of the Electrocatalytic CO2 Reduction on Graphene-Embedded Fe-N-C Motifs: Bridging Concepts between Molecular Homogeneous and Solid-State Heterogeneous Catalysis. *ACS Energy Lett.* **3**, 812–817 (2018).
9. Wuttig, A., Yaguchi, M., Motobayashi, K., Osawa, M. & Surendranath, Y. Inhibited proton

transfer enhances Au-catalyzed CO 2 -to-fuels selectivity. *Proc. Natl. Acad. Sci.* **113**, E4585–E4593 (2016).

10. Verma, S. *et al.* Insights into the Low Overpotential Electroreduction of CO 2 to CO on a Supported Gold Catalyst in an Alkaline Flow Electrolyzer. (2017). doi:10.1021/acsenergylett.7b01096

11. Prslja, P. & López, N. Stability and Redispersion of Ni Nanoparticles Supported on N-Doped Carbons for the CO2Electrochemical Reduction. *ACS Catalysis* **11**, 88–94 (2021).

12. Dunwell, M. *et al.* The Central Role of Bicarbonate in the Electrochemical Reduction of Carbon Dioxide on Gold. *J. Am. Chem. Soc.* **139**, 3774–3783 (2017).

13. Hansen, H. A., Varley, J. B., Peterson, A. A. & Nørskov, J. K. Understanding trends in the electrocatalytic activity of metals and enzymes for CO2 reduction to CO. *J. Phys. Chem. Lett.* **4**, 388–392 (2013).

14. Chen, L. D., Urushihara, M., Chan, K. & Nørskov, J. K. Electric Field Effects in Electrochemical CO2 Reduction. *ACS Catal.* **6**, 7133–7139 (2016).

15. Limaye, A. M., Zeng, J. S., Willard, A. P. & Manthiram, K. Bayesian data analysis reveals no preference for cardinal Tafel slopes in CO2 reduction electrocatalysis. *Nat. Commun.* **12**, 1–10 (2021).

16. Hori, Y., Wakebe, H., Tsukamoto, T. & Koga, O. Electrocatalytic process of CO selectivity in electrochemical reduction of CO2 at metal electrodes in aqueous media. *Electrochim. Acta* **39**, 1833–1839 (1994).

17. Brown, S. M. *et al.* Electron Transfer Limitation in Carbon Dioxide Reduction Revealed by Data-Driven Tafel Analysis. *ChemRxiv* (2020). doi:10.26434/chemrxiv.13244906.v1

18. Ju, W. *et al.* Unraveling Mechanistic Reaction Pathways of the Electrochemical CO2

Reduction on Fe-N-C Single-Site Catalysts. *ACS Energy Lett.* **4**, 1663–1671 (2019).

19. Benson, E. E., Kubiak, C. P., Sathrum, A. J. & Smieja, J. M. Electrocatalytic and homogeneous approaches to conversion of CO2to liquid fuels. *Chem. Soc. Rev.* **38**, 89–99 (2009).

20. Göttle, A. J. & Koper, M. T. M. Proton-coupled electron transfer in the electrocatalysis of CO2 reduction: prediction of sequential vs. concerted pathways using DFT. *Chem. Sci.* **8**, 458–465 (2016).

21. Gennaro, A. *et al.* Mechanism of the electrochemical reduction of carbon dioxide at inert electrodes in media of low proton availability. *J. Chem. Soc. - Faraday Trans.* **92**, 3963–3968 (1996).

22. Zhang, B. A., Costentin, C. & Nocera, D. G. Driving force dependence of inner-sphere electron transfer for the reduction of CO2on a gold electrode. *J. Chem. Phys.* **153**, (2020).

23. Ringe, S. *et al.* Double Layer Charging Driven Carbon dioxide Adsorption Limits the Rate of Electrochemical Carbon dioxide Reduction on Gold. *Nat. Commun.* **11**, (2020).

24. Vijay, S. *et al.* Dipole-field interactions determine the CO2 reduction activity of 2D Fe-N-C single atom catalysts. *ACS Catal.* **57**, 13 (2020).

25. Gauthier, J. A. *et al.* Facile Electron Transfer to CO2 during Adsorption at the Metal|Solution Interface. *J. Phys. Chem. C* **123**, 29278–29283 (2019).

26. Verma, A. M., Honkala, K. & Melander, M. M. Computational Screening of Doped Graphene Electrodes for Alkaline CO2 Reduction. *Front. Energy Res.* **8**, 388 (2021).

27. Brown, S. M. *et al.* Electron Transfer Limitation in Carbon Dioxide Reduction Revealed by Data-Driven Tafel Analysis. *ChemRxiv* (2020). doi:10.26434/chemrxiv.13244906.v1

28. Gauthier, J. A. *et al. Facile Electron Transfer to CO2 during Adsorption at the*

Metal|Solution Interface. *Journal of Physical Chemistry C* **123**, (ChemRxiv, 2019).

29. Newns, D. M. Self-consistent model of hydrogen chemisorption. *Phys. Rev.* **178**, 1123–1135 (1969).

30. Anderson, P. W. Localized magnetic states in metals. *Phys. Rev.* **124**, 41–53 (1961).

31. Grimley, T. B. Overlap effects in the theory of adsorption using Anderson's Hamiltonian. *J. Phys. C Solid State Phys.* **3**, 1934–1942 (1970).

32. Gauthier, J. A. *et al.* Challenges in Modeling Electrochemical Reaction Energetics with Polarizable Continuum Models. *ACS Catal.* **9**, 920–931 (2019).

33. Nørskov, J. K., Studt, F., Abild-Pedersen, F. & Bligaard, T. *Fundamental Concepts in Heterogeneous Catalysis*. *Fundamental Concepts in Heterogeneous Catalysis* **9781118888**, (Wiley Blackwell, 2014).

34. Hansen, H. A., Viswanathan, V. & NØrskov, J. K. Unifying kinetic and thermodynamic analysis of 2 e- and 4 e - reduction of oxygen on metal surfaces. *J. Phys. Chem. C* **118**, 6706–6718 (2014).

35. Limmer, D. T., Willard, A. P., Madden, P. & Chandler, D. Hydration of metal surfaces can be dynamically heterogeneous and hydrophobic. *Proc. Natl. Acad. Sci. U. S. A.* **110**, 4200–4205 (2013).

36. Huang, B. *et al.* Cation-Dependent Interfacial Structures and Kinetics for Outer-Sphere Electron-Transfer Reactions. *J. Phys. Chem. C XXXX* **18**, 2021

37. Gu, J., Hsu, C. S., Bai, L., Chen, H. M. & Hu, X. Atomically Dispersed Fe3+ Sites Catalyze Efficient CO2 Electroreduction to CO. *Science (80-.).* **364**, 1091–1094 (2019).

38. Mortensen, J. J., Hammer, B. & Nørskov, J. K. Alkali promotion of N2 dissociation over Ru(0001). *Phys. Rev. Lett.* **80**, 4333–4336 (1998).

39. Marshall-Roth, T. *et al.* A pyridinic Fe-N4 macrocycle models the active sites in Fe/N-doped carbon electrocatalysts. *Nat. Commun.* **11**, 1–14 (2020).

40. Hansen, H. A., Varley, J. B., Peterson, A. A. & Nørskov, J. K. Understanding trends in the electrocatalytic activity of metals and enzymes for CO2 reduction to CO. *J. Phys. Chem. Lett.* **4**, 388–392 (2013).

41. Luo, F. *et al.* Accurate Evaluation of Active-Site Density (SD) and Turnover Frequency (TOF) of PGM-Free Metal-Nitrogen-Doped Carbon (MNC) Electrocatalysts using CO Cryo Adsorption. *ACS Catal.* **9**, 4841–4852 (2019).

42. Kramm, U. I. *et al.* Structure of the catalytic sites in Fe/N/C-catalysts for O 2-reduction in PEM fuel cells. *Phys. Chem. Chem. Phys.* **14**, 11673–11688 (2012).

43. Jiang, K. *et al.* Transition-Metal Single Atoms in a Graphene Shell as Active Centers for Highly Efficient Artificial Photosynthesis. *Chem* **3**, 950–960 (2017).

44. Jiang, K. *et al.* Isolated Ni single atoms in graphene nanosheets for high-performance CO2 reduction. *Energy Environ. Sci.* **11**, 893–903 (2018).

45. Luo, F. *et al.* Surface site density and utilization of platinum group metal (PGM)-free Fe-NC and FeNi-NC electrocatalysts for the oxygen reduction reaction. *Chem. Sci.* **12**, 384–396 (2021).

46. Vojvodic, A., Nørskov, J. K. & Abild-Pedersen, F. Electronic structure effects in transition metal surface chemistry. *Top. Catal.* **57**, 25–32 (2014).

47. Greiner, M. T. *et al.* Free-atom-like d states in single-atom alloy catalysts. *Nat. Chem.* **10**, 1008–1015 (2018).

48. Thirumalai, H. & Kitchin, J. R. Investigating the Reactivity of Single Atom Alloys Using Density Functional Theory. *Top. Catal.* **61**, 462–474 (2018).

49. Larsen, A. H., Kleis, J., Thygesen, K. S., Nørskov, J. K. & Jacobsen, K. W. Electronic shell structure and chemisorption on gold nanoparticles. *Phys. Rev. B - Condens. Matter Mater. Phys.* **84**, 1–13 (2011).

50. Li, L. *et al.* Investigation of Catalytic Finite-Size-Effects of Platinum Metal Clusters. *J. Phys. Chem. Lett* **4**, 6 (2013).

51. Ji, Y., Nørskov, J. K. & Chan, K. Scaling relations on basal plane vacancies of transition metal dichalcogenides for co 2 reduction. *J. Phys. Chem. C* **123**, 4256–4261 (2019).

52. Kim, D., Shi, J. & Liu, Y. Substantial Impact of Charge on Electrochemical Reactions of Two-Dimensional Materials. *J. Am. Chem. Soc.* **140**, 9127–9131 (2018).

53. Zhao, X. & Liu, Y. Unveiling the Active Structure of Single Nickel Atom Catalysis: Critical Roles of Charge Capacity and Hydrogen Bonding. *J. Am. Chem. Soc.* **142**, 5773–5777 (2020).

54. Singh, A. R. *et al.* Computational Design of Active Site Structures with Improved Transition-State Scaling for Ammonia Synthesis. *ACS Catal.* **8**, 4017–4024 (2018).

55. Birdja, Y. Y. *et al.* Advances and challenges in understanding the electrocatalytic conversion of carbon dioxide to fuels. doi:10.1038/s41560-019-0450-y